Electronic, Structural, and Reactive Properties of Ultrathin Aluminum Oxide Films on Pt(111)

Karen Wilson, Adam F. Lee,† Christopher Hardacre,‡ and Richard M. Lambert*

Department of Chemistry, University of Cambridge, Cambridge, CB2 1EW, England

Received: September 26, 1997; In Final Form: December 8, 1997

Low-energy electron diffraction, X-ray photoelectron spectroscopy, high-resolution electron energy-loss spectroscopy, scanning tunneling microscopy, and temperature-programmed reaction spectrometry results are reported for the structural and reactive behavior of alumina films grown on Pt(111) as a function of thickness and oxidation temperature. Submonolayer Al films undergo compete oxidation at 300 K, annealing at 1100 K resulting in formation of somewhat distorted crystalline γ-alumina. Thicker deposits require 800 K oxidation to produce Al_2O_3, and these too undergo crystallization at 800 K, yielding islands of apparently undistorted γ-alumina on the Pt(111) surface. Oxidation of a $p(2 \times 2)$ Pt_3Al surface alloy occurs only at >800 K, resulting in Al extraction. These alumina films on Pt(111) markedly increase the coverage of adsorbed SO_4 resulting from SO_2 chemisorption onto oxygen-precovered surfaces. This results in enhanced propane uptake and subsequent reactivity relative to SO_4/Pt(111). A bifunctional mechanism is proposed to account for our observations, and the relevance of these to an understanding of the corresponding dispersed systems is discussed.

Introduction

Pt/Al_2O_3 is one of the most widely used and intensively studied catalytic systems finding extensive applications in a number of important fields, including pollution abatement[1] and large-scale hydrocarbon processing.[2] Al_2O_3, normally considered a nonreducible support, does exhibit a strong metal−support interaction after ~1000 K reduction in H_2. This has been attributed to formation of a Pt−Al alloy at the metal/oxide interface.[3] Subsequent oxidation results in loss of active Pt area, an effect ascribed to Al_2O_3 growth on top of Pt clusters.[3] A relevant earlier paper[4] described the structural and thermal properties of Al films grown on Pt(111). However, it remains true that there is relatively little fundamental understanding of the Pt−Al−Al_2O_3 interface. In this paper we describe the structural and electronic properties of a model system consisting of Al_2O_3 overlayers grown on Pt(111). The reactive behavior of this system in the SO_2-promoted oxidation of propane is also reported. This reaction is of major importance in the control of automobile emissions by conventional exhaust catalysts. Any unburnt hydrocarbons (mainly C_3) present in the exhaust stream must be selectively combusted to CO_2 at high conversion. The rate-limiting step in propane combustion is C−H bond cleavage, making oxidation much less efficient than observed for the unsaturated equivalent, propene, where direct interaction of the C−C π bond with oxygen can occur.[5] In the presence of SO_2, however, significant promotion of propane oxidation has been observed over Pt/Al_2O_3 catalysts.[6,7]

The origin of SO_2 promotion of propane oxidation over dispersed Pt/alumina catalysts[6,7] was previously poorly understood. We studied SO_2-promoted propane oxidation over Pt(111) under ultrahigh vacuum (UHV) conditions *in the absence of alumina*,[8] demonstrating that SO_4(a) is the key surface species that leads to dissociative chemisorption and subsequent oxidation of hydrocarbon molecules impinging on the metal surface.[9] To understand the role of Al_2O_3 in this catalytic process, the growth of alumina films on Pt(111) and their reactivity in SO_2-promoted propane oxidation have been investigated by temperature-programmed reaction spectrometry (TPRS), high-resolution electron energy-loss spectroscopy (HREELS), Auger electron spectroscopy (AES), X-ray photoelectron spectroscopy (XPS), low-energy electron diffraction (LEED), and scanning tunneling microscopy (STM). By this means, we hope to eliminate complicating effects that can arise with dispersed catalysts due to variations in Pt particle size. Such effects are large in the SO_2-promoted oxidation of propane over dispersed Pt/alumina catalysts.[10]

Experimental Methods

Photoemission and HREELS experiments were carried out in a VSW ARIES ultrahigh vacuum chamber, operated at base pressures of 1×10^{-10} Torr.[11] The Pt(111) sample could be resistively heated to 1200 K and cooled to 150 K. Cleaning was achieved by cycles of Ar^+ sputtering (6×10^{-2} A m^{-2}, 500 eV) and annealing at 1000 K until LEED/Auger/XPS analysis indicated a well-ordered surface free from contaminants. Oxygen treatment (800 K, 1×10^{-8} Torr) followed by thermal desorption was used as a sensitive test for the absence of C, which is diagnosed by subsequent desorption of O_2 and the absence of CO or CO_2 desorption. X-ray photoelectron spectra were obtained using a VSW HA100 spectrometer with both analyzer and excitation (Mg Kα) source at 45° to the surface normal. HREEL spectra were recorded in the specular direction using a VSW HA300 instrument with an incident beam energy of 9.6 eV and resolution of ~95 cm^{-1}. STM measurements were carried out with an Omicron UHV VT-STM system (base pressure of 4×10^{-11} Torr) equipped with LEED and AES capabilities. Images were acquired at 300 K in constant-current (topographic) mode with an electrochemically etched W tip

* Corresponding author: rml1@cam.ac.uk.
† Department of Chemistry, University of Hull, Hull, HU6 7RX, England.
‡ School of Chemistry, Queen's University, Belfast BT9 5AG, Northern Ireland.

S1089-5647(97)03134-9 CCC: $15.00
Published on Web 02/12/1998

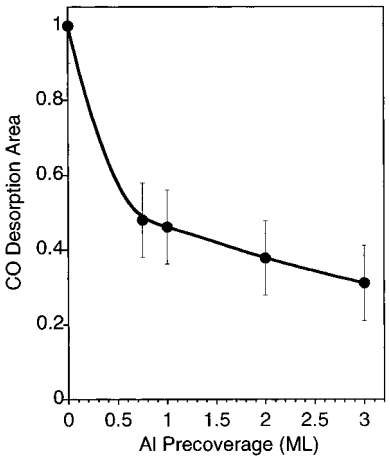

Figure 1. CO titration (25-L exposure) of 300 K oxidized Al films on Pt(111) as a function of Al film thickness. Oxidation was performed with 300 L of O_2 at 300 K.

biased between ±100 mV and ±2 V with tunnel currents from 0.5 to 5 nA.

TPRS, LEED, and AES measurements were made in a third chamber equipped with a three-grid retarding field analyzer (RFA) for LEED and Auger analyses and a quadrupole mass spectrometer (VG) for TPRS experiments. This has been described in detail elsewhere.[12] TPRS experiments were performed using a capillary array doser to expose the sample sequentially to O_2 (99.995%), SO_2 (99.98%), and C_3H_8 (99.95%) (all supplied by M. G. Distillers) at 300 K prior to heating the sample to 1000 K at a rate of 17 K s^{-1}. During TPRS/temperature-programmed desorption (TPD) experiments, the front face of the sample could be positioned ~2 mm from the collimator fitted to the mass-spectrometer ionizer. Control experiments showed that >90% of the detected signal was due to molecules beamed directly from the sample front face to the ionizer with ~10% of the signal due to scattered gas. Al (Goodfellows 99.99%) was deposited using a well-collimated evaporation source described previously.[13] This provided highly reproducible deposition rates of ~0.15 monolayer (ML) per minute. A monolayer is defined as 1.5×10^{-15} adatoms cm^{-2}, i.e., equal to the atomic density of the Pt(111) surface. (One monolayer of Al results in a 50% attenuation of the Pt 43-eV Auger signal.[4]) Only the front face of the sample was dosed with Al. Oxidation of Al films and Pt−Al alloys was performed at pressures of 1×10^{-7} Torr at 300 and 800 K. Following 800 K oxidation the sample was cooled to 300 K over a period of ~5 min in a background O_2 pressure of 1×10^{-7} Torr.

Results

Characterization of AlO_x Film Growth on Pt(111). *i. CO Titration of Pt Sites after Deposition of Alumina.* The growth of Al films on Pt(111) has been well characterized in our laboratory;[4] hence, Al films having well-defined thickness could be deposited by appropriate scaling of the deposition time required to form a complete film. Oxidation of these films was then performed at 300 K using a maximum oxygen exposure of 300 L. The remaining bare Pt sites were then titrated as a function of predeposited Al film thickness (0−3 ML) by exposing the surface to a saturation (25 L) CO exposure at 300 K. The resulting CO TPD yield provided a measure of residual Pt surface area. Figure 1 shows the integrated CO desorption yield as a function of AlO_x loading. It can be seen that this decreases to about 50% of the clean Pt(111) value for ~0.75-ML films. A further decrease in the number of titratable Pt sites is observed up to 3 ML of AlO_x; however, ~20−30% of Pt sites remain uncovered, indicating that these multilayer AlO_x films consist of islands. The estimated uncertainty is due to the possible contribution from CO desorption off the (deliberately) contaminated back face of the crystal (see Experimental Methods).

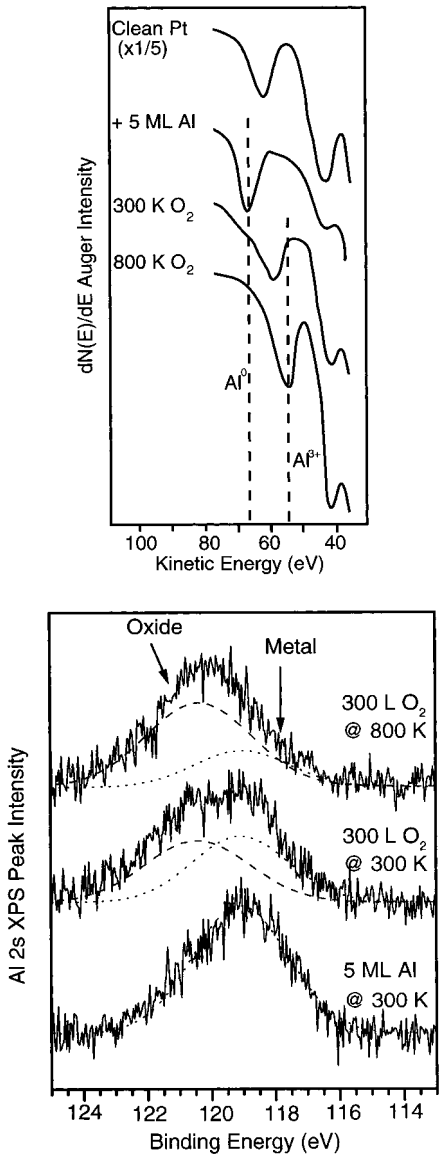

Figure 2. (a, top) AES and (b, bottom) Al 2s XP spectra following 300 K deposition of 5 ML of Al onto Pt(111) and exposure to 300 L of O_2 at 300 K and then at 800 K. Deconvoluted metallic and oxidic Al 2s components are also shown.

ii. Auger and X-ray Photoelectron Spectroscopy. The variation in oxidation state of Al films (0−5 ML) grown on Pt(111) was followed after exposure to 1×10^{-7} Torr O_2 at 300 and 800 K using AES and XPS. Chemical shifts in the 66-eV Al LMM Auger transition provide a key means of fingerprinting the oxidation state of Al, with shifts up to 14 eV being observed between Al^0 and Al^{3+}.[14] However, for this system, overlap of the Al 66-eV and Pt 64-eV NVV Auger transitions precludes observation of the Al Auger emission except for thick Al films (>5 ML) for which the Pt emission was totally quenched. Figure 2a shows the Al 66-eV Auger intensities after deposition of 5 ML of Al onto Pt(111) at 300 K. Subsequent sequential oxidation of the film first at 300 K and then at 800 K shifted the Al transition to 57 and 54 eV, respectively.

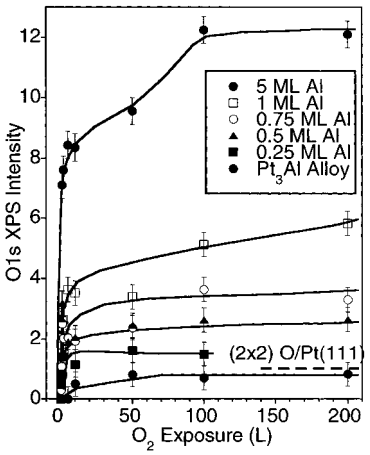

Figure 3. Integrated O 1s XPS intensities following 300 K oxygen uptakes over 0.25−5-ML Al films and a Pt_3Al alloy. The corresponding O 1s intensity for the 0.25-ML $p(2 \times 2)$-O/Pt(111) surface is also shown for reference.

Al film oxidation was also monitored via the Al 2s X-ray photoelectron (XP) signal, chosen in preference to the more intense Al 2p signal that overlaps with the Pt 4f XP transitions. Figure 2b shows the effect on the Al 2s signal of first 300 K and then 800 K oxidation of a 5-ML Al film. After a 300-L O_2 exposure at 300 K, the initial metallic Al transition centered at 119-eV binding energy (BE) exhibits a high-energy shoulder at 120.5 eV. Oxidation by a subsequent 300-L O_2 dose at 800 K gave further changes in line shape until the Al 2s transition was eventually centered at 120.5 eV. The low absorption cross section of the Al 2s level with Mg Kα radiation prohibited similar measurements on thinner Al films (<5 ML).

The oxidation of Al films and of the $p(2 \times 2)$ Pt_3Al surface alloy (prepared by annealing a 3-ML Al film to 800 K) was also studied by following the intensity of the O 1s XP signal as a function of exposure at 300 K. In each case, the 300 K oxygen-saturated film was subsequently exposed to 300 L of O_2 at 800 K followed by XP analysis. This second treatment had no effect on submonolayer Al deposits but significantly increased the oxygen uptake of thicker films while drastically increasing oxygen uptake by the $p(2 \times 2)$-Pt_3Al surface alloy (see below). Oxidation of (i) 0.25−5-ML Al films and (ii) the $p(2 \times 2)$-Pt_3Al surface alloy was examined to investigate the effects of film thickness and of the extent of Al−Pt interaction, respectively, on the oxidation process. Figure 3 illustrates the integrated O 1s intensities, which show rapid initial growth with increasing oxygen exposure, saturating after ~20 L for submonolayer films and ~100 L for a 5-ML film. Note that the limiting O 1s signal scales approximately with Al loading between 0.25 and 1.0 ML. The O 1s signal for oxygen-saturated clean Pt(111) ($\theta(O_a) = 0.25$ ML) is shown for comparison. Clearly, the Pt_3Al surface alloy is resistant to 300 K oxidation and exhibits a limiting O 1s signal comparable to that of oxygen-saturated Pt(111).

Evidence for the incomplete oxidation of thick Al films is provided by the Al 2s XP spectra. Figure 2b shows the Al 2s signal for a 5-ML Al film that has been oxidized at 300 and 800 K. Deconvolution of these spectra shows that some Al remains in metallic form even after a "saturation" exposure at 300 K. Peak fitting was performed using Gaussian functions for both the metallic and oxidic Al components, with parameters for the metallic state determined from the unoxidized Al deposits. Complete oxidation of Al films to Al^{3+} is expected to increase the Al 2s BE by 1.5−2 eV,[15] consistent with the oxide contribution observed after 300 K saturation oxygen

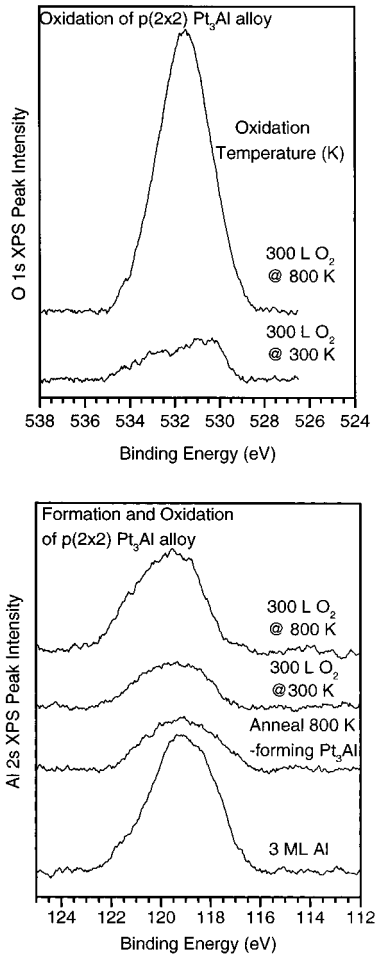

Figure 4. (a, top) O 1s XP spectra following exposure of a $p(2 \times 2)$ Pt_3Al alloy to 300 L of O_2 first at 300 K, then at 800 K. (b, bottom) Al 2s XP spectra following deposition of 3 ML of Al at 300 K followed by annealing to 800 K to form the $p(2 \times 2)$ Pt_3Al alloy and subsequent oxidation by 300 L of O_2 first at 300 K, then at 800 K.

exposure. Similar deconvolution of the Al 2s signal following 800 K oxidation indicates that most of the Al (~80%) is now present in an oxidic state, with a BE ~1.8 eV higher than that of the as-deposited (119 eV) metallic film. The associated 70% increase in the O 1s signal at 800 K relative to the 300 K oxidized surface is in accord with this.

The most dramatic effect of oxidation temperature was observed for the (2×2)-Pt_3Al alloy for which the limiting O 1s intensity following a 300-L O_2 exposure increases 10-fold between 300 and 800 K (Figure 4a). The intensity of the Al 2s emission *also increased* during 800 K oxidation of the Pt_3Al alloy, indicating extraction of Al from the mixed Pt/Al contact layer. This is illustrated in Figure 4b, which shows Al 2s XP spectra acquired during Al deposition, alloy formation, and subsequent oxidation.

In this connection, it is important to recall our earlier finding that 300 K deposition of Al on Pt(111) results in Pt/Al mixing in the contact layer *only for film thickness in excess of 1 ML*; submonolayer films exhibit a sharp Pt/Al interface.[4] Pt/Al intermixing is accompanied by a Pt core level BE shift of ~1 eV. Parts a and b of Figure 5 show the Pt 4d and valence band spectra, respectively, for the clean surface after deposition of a 5-ML Al film, oxidation at 300 K, and then further oxidation at 800 K. After the 300 K oxidation the Pt 4d and valence features exhibit only slight broadening to lower binding energies. In contrast, oxidation at 800 K proved sufficient to restore both Pt 4d and valence spectra to their clean surface condition.

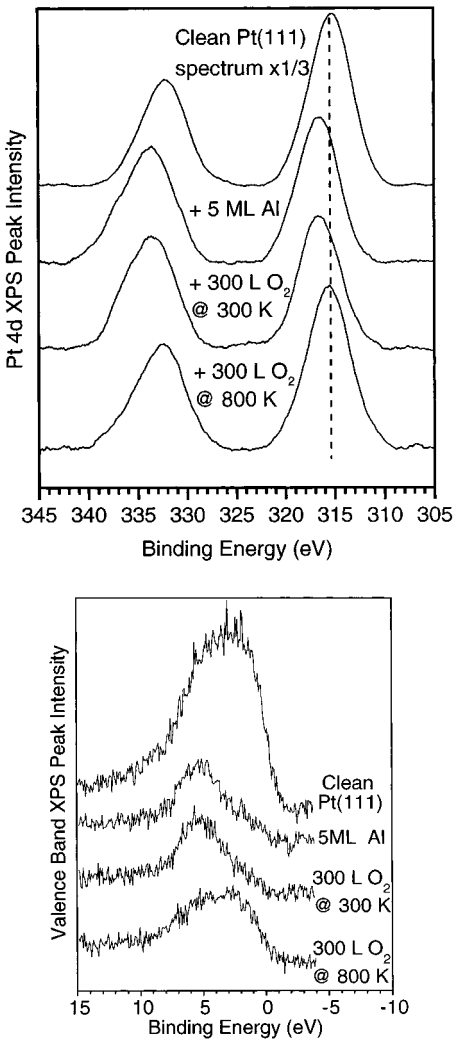

Figure 5. (a, top) Pt 4d XP spectra following deposition of 5 ML of Al and subsequent oxidation by 300 L of O_2 at 300 K and then at 800 K. Note the clean surface spectrum is scaled by $^1/_3$. (b, bottom) Valence-band XP spectra following deposition of 5 ML of Al and subsequent oxidation by 300 L of O_2 at 300 K and then at 800 K.

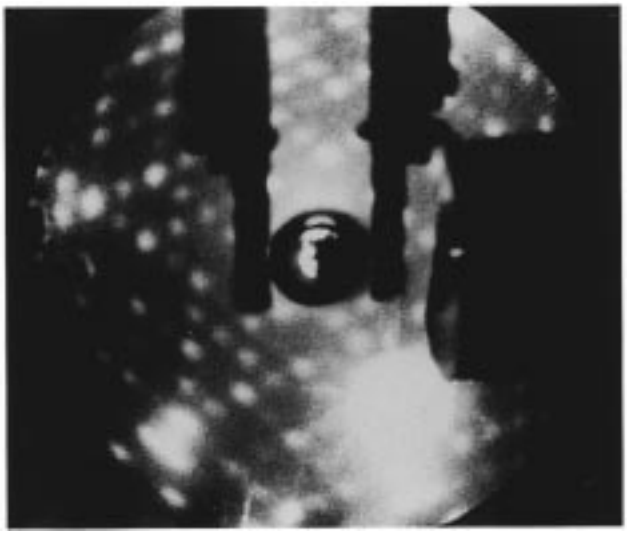

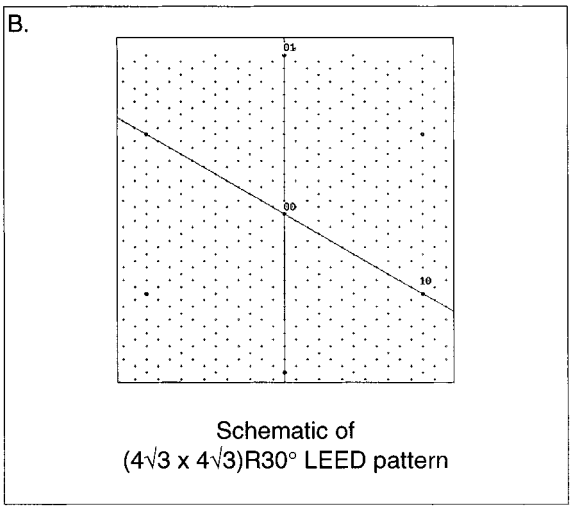

Figure 6. (A, top) $(4\sqrt{3} \times 4\sqrt{3})R30°$ LEED pattern (at 68.8 eV) obtained following 300 K oxidation of 0.25 ML of Al film grown on Pt(111) and subsequent 1100 K annealing. (B, bottom) Schematic of $(4\sqrt{3} \times 4\sqrt{3})R30°$ LEED pattern (rotated by 30° with respect to the pattern in part A).

iii. LEED. No new ordered structures were observed upon 300 K oxidation of any Al film; for thick Al films (>5 ML), 800 K oxidation resulted in a diffuse (1 × 1) LEED pattern corresponding to a lattice parameter of ~2.8 Å. Likewise, 800 K oxidation of the (2 × 2)-Pt_3Al alloy gave only a diffuse (1 × 1) pattern. However, when thin (<0.5 ML) 300 K oxidized Al films were annealed to 1100 K, the complex LEED pattern shown in Figure 6A appeared. This pattern, which derives from a $(4\sqrt{3} \times 4\sqrt{3})R30°$ mesh, is shown schematically in Figure 6B. For thicker oxidized films, annealing to 1100 K gave only the diffuse (1 × 1) pattern.

iv. HREELS. Figure 7 shows HREEL spectra recorded following oxidation of 0.5- and 5-ML Al films deposited on Pt(111) at 300 K, after subsequent annealing to 1100 K, and after further oxidation at 800 K, respectively. No losses were detectable after 300 K oxidation of the thick and thin films. However, when both films were annealed to 1100 K (the temperature at which the $(4\sqrt{3} \times 4\sqrt{3})R30°$ LEED pattern evolves for the 0.5-ML film), well-defined losses appeared in the range 300−900 cm^{-1}. For the thin oxidized Al film a strong mode appeared at 870 cm^{-1} accompanied by two weaker modes at 450 and 670 cm^{-1}, while the 5-ML film exhibits a single broad band centered at 650 cm^{-1}. Upon further oxidation of this 5-ML film at 800 K, the mode at 650 cm^{-1} increased in intensity and a weaker loss at 820 cm^{-1} appeared.

v. Scanning Tunneling Microscopy. Oxidation of submonolayer Al films was followed using STM by exposure of the surface to O_2 while in the STM stage. Parts A and B of Figure 8 show the topography of a 0.25-ML Al film grown on Pt(111) at 300 K before and after exposure to 100 L of O_2 at 300 K. It can be seen that prior to O_2 exposure Al forms 2D dendritic islands on Pt(111). Subsequent oxidation induced significant (~5−10%) expansion of the Al dendrites in the surface plane, i.e., spreading. In some areas this spreading led to coalescence of neighboring islands. However, the overall island shape remains dendritic, and thus, a larger Pt−Al_2O_3 perimeter was maintained than would if compact Al_2O_3 islands had formed. This diffusion-limited growth may prove important in determining the chemistry at the Pt−Al_2O_3 boundary (i.e., metal−support spillover phenomena). Oxidation at 300 K of thicker films led to an overall increase in surface roughness without the appearance of striking, new topographical features. Oxidation of the tip during such experiments also led to a degradation of image quality. Oxidation at 800 K could not be studied because of instrumental limitations.

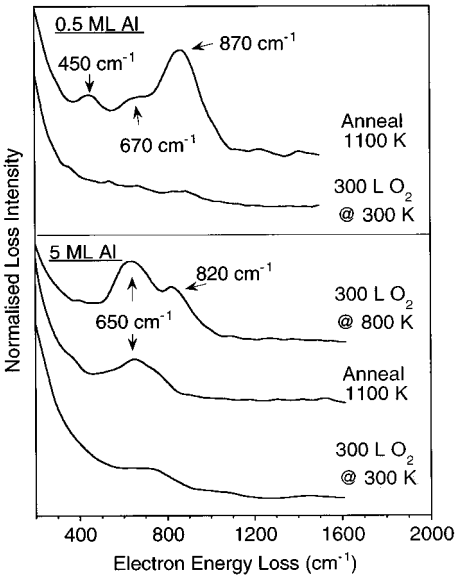

Figure 7. HREELS following (i) exposure of a 0.5-ML Al film on Pt(111) to 300 L of O_2 at 300 K and then annealing to 1100 K and (ii) exposure of a 5-ML Al film on Pt(111) to 300 L of O_2 at 300 K followed by annealing to 1100 K and then exposure to 300 L of O_2 at 800 K.

Reactivity of Sulfated AlO_x Films. *i. Temperature-Programmed Reaction.* To elucidate the possible catalytic role of alumina in dispersed Pt/alumina catalysts, SO_2-promoted oxidation of propane was investigated over AlO_x/Pt(111) surfaces generated by 300 K oxidation of Al films. Only Al films in the range 0−3 ML were investigated, since the preceding structural characterization shows these overlayers are fully oxidized. At 300 K and for doses up to 100 L, propane chemisorption is undetectable on oxygen-precovered Pt(111) surfaces in the absence of preadsorbed (oxygen + SO_2).[8] Here, we again find that in the absence of SO_2 preadsorption the oxygenated AlO_x/Pt(111) surface is equally inert to propane adsorption. However, sequential exposure of this surface to 100 L of O_2, 24 L of SO_2, and 6 L of C_3H_8 at 300 K (conditions for which significant propane oxidation is observed over clean Pt-(111)[8]) did result in dissociative chemisorption of propane. Subsequent TPRS sweeps showed the evolution of combustion products. Representative results for a 0.5-ML alumina film are shown in Figure 9. Water desorption from Pt(111) has been shown to occur below 300 K [16] and is only observed if propane exposures is performed at 160 K.[8] The absence of H_2O under the conditions of this experiment can thus be accounted for by the immediate desorption of reactively formed H_2O below 300 K. In principle it is possible to follow the production of H_2O during propane exposure; however, this could not be performed in this study because of limitations of the experimental geometry.

Integrated product desorption yields are shown in Figure 10 as a function of increasing AlO_x film thickness. As the AlO_x coverage increases, both propane conversion and the selectivity toward partial versus total oxidation products initially rise, showing maxima at ∼1 ML. The presence of increasing amounts of AlO_x progressively modifies the SO_2 desorption profile, as shown in Figure 11. Over clean Pt(111) alone the sequential adsorption of 100 L of O_2, 24 L of SO_2 followed by 6 L of C_3H_8 results in two SO_2 desorption peaks at 400 and 550 K. The 550 K peak is assigned to the 64-amu fragment ion (SO_2^+) of SO_3 desorbing from Pt.[9] As the AlO_x film thickness increases from 0.5 to 1.0 ML, the intensity of the 550 K (SO_3) peak decreases while a new, broad peak emerges between 550 and 750 K. As discussed below, we assign this to desorption of sulfoxy species (SO_4(a)) located at the Pt−AlO_x interface. For films greater than 2.0 ML, increases in AlO_x

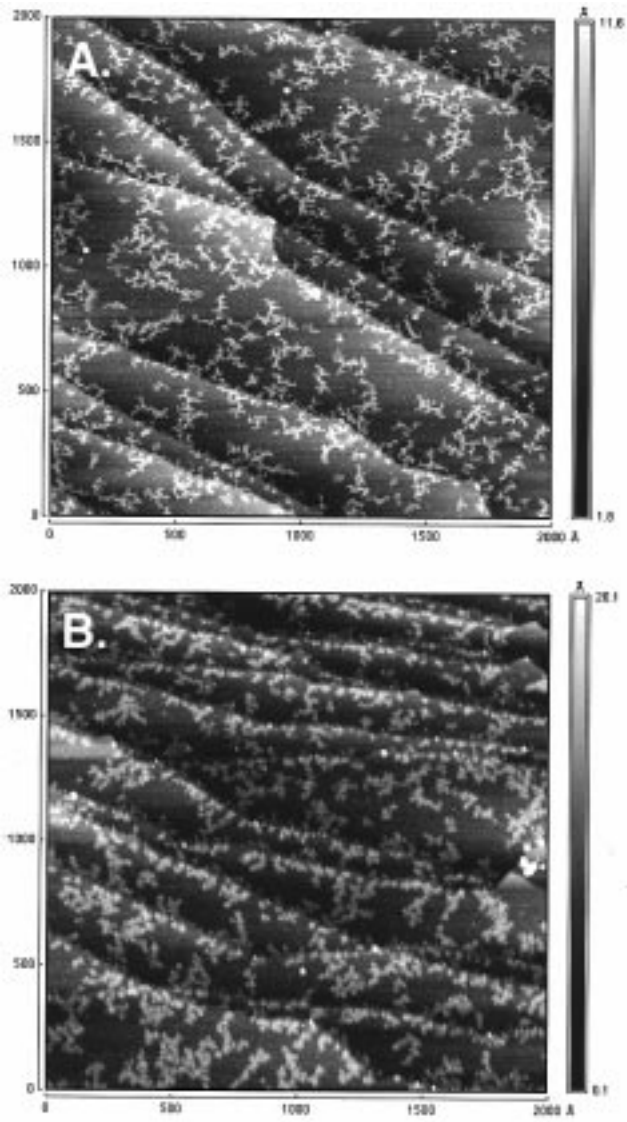

Figure 8. (A) STM following deposition of 0.25 ML of Al onto Pt-(111) at 300 K. (B) STM following exposure of the 0.25-ML Al film to 100 L of O_2 at 300 K.

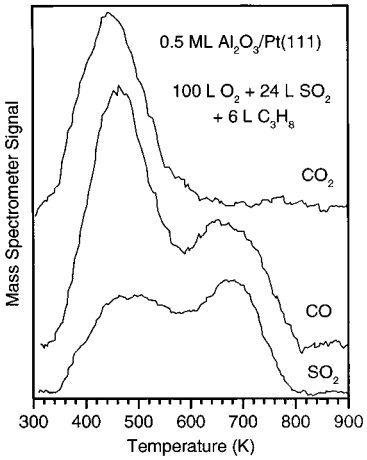

Figure 9. TPRS following sequential exposure of a 0.5-ML Al_2O_3 film grown on Pt(111) at 300 K to 100 L of O_2 + 24 L of SO_2 + 6 L of C_3H_8 at 300 K.

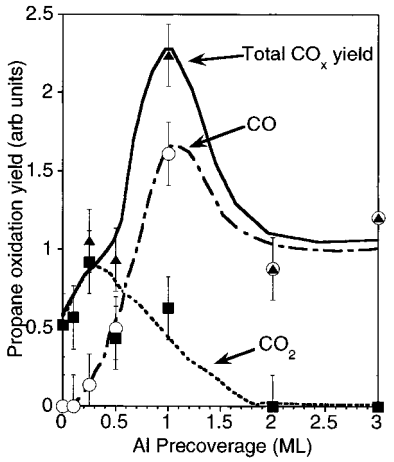

Figure 10. Integrated CO and CO_2 yields following sequential exposure of Al_2O_3 films (0−3 ML) grown on Pt(111) to 100 L of O_2 + 24 L of SO_2 + 6 L of C_3H_8 at 300 K.

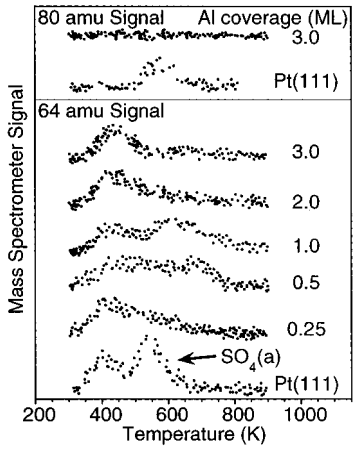

Figure 11. Mass spectrometer signals at 64 and 80 amu obtained following reaction of 100 L of O_2 + 24 L of SO_2 + 6 L of C_3H_8 over Al_2O_3 films (0−3 ML) grown on Pt(111) at 300 K.

film thickness attenuate this species, leaving a single broad desorption at ∼400 K. This is characteristic of SO_2 desorption from both Pt(111)[9] and from Al_2O_3 powder.[17]

ii. X-ray Photoelectron Spectroscopy. S 2p XP spectra were recorded after 300 K exposure of AlO_x films to 100 L of O_2 and 50 L of SO_2 as a function film thickness (Figure 12). On clean Pt(111), surfaces pretreated in this way are active for C_3H_8 dissociative chemisorption, an effect that is induced by the presence of SO_4.[8,9,18] However, this species is unstable with respect to electron-stimulated dissociation[9,19] so that XP spectra of sulfated clean Pt(111) show only a weak emission at 164.5 eV BE, similar to the S 2p state resulting from 300 K adsorption of H_2S.[9] This emission is attributed to atomic sulfur (S_a) resulting from electron-stimulated decomposition (ESD) of adsorbed SO_4, which occurs on the metal surface during the time scale of the XPS experiments.[9,19] However, in the presence of 0.5 ML of AlO_x, two S species were observed at ∼164.5 and ∼170 eV BE, respectively. The former is again assigned to S_a, while comparison with literature data[9,20] suggests that the latter state corresponds to an SO_4 species. The increase of the S_a state with Al_2O_3 coverage indicates that although ESD of the SO_4 species present on both Pt and Al_2O_3 occurs, the SO_4 species formed on Al_2O_3 films are more stable than those on the Pt(111) substrate. This assignment is confirmed by the results shown in Figure 12 from which it is apparent that increasing the amount of AlO_x increases the population of both species.

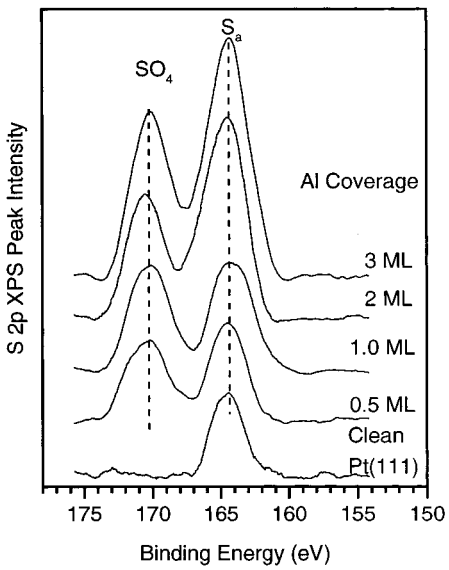

Figure 12. S 2p XP spectra following sequential 300 K exposure of Al_2O_3 films (0−3 ML) grown on Pt(111) at 300 K to 100 L of O_2 + 24 L of SO_2.

Discussion

i. Morphology of AlO_x Films. The evolution of α-alumina from γ-alumina precursors is a complex process involving a variety of intermediate structures sharing a common stoichiometry[21] of which the γ- and α-Al_2O_3 forms are the most commonly used as catalyst supports. Oxidation of Al is highly exothermic (ΔH_f = −1690.7 kJ mol^{-1} [22]), with kinetics controlled by the transport of oxygen.[23] Oxidation of thin Al films is thus expected to exhibit a dependence on Al film thickness. By studying this, one might hope to determine the influence of Pt on the oxidation kinetics of Al and conditions for the formation of crystalline oxide overlayers.

Room-temperature oxygen exposure of Al films results in oxygen uptake beyond the saturation coverage possible on clean Pt(111) ($\theta(O_a)$ = 0.25 ML). This must be associated with Al oxidation. It is known that oxidation of Al(111) to yield Al^{3+} is accompanied by an increase in Al 2p BE of 2.5−2.7 eV.[24] This is considerably higher than the shifts associated with chemisorbed oxygen adlayers on Al{111}, i.e., 0.37, 0.84, and 1.37 eV, reflecting Al coordination to one, two, and three oxygen atoms respectively.[24] In the present case, both 300 and 800 K oxidation of a 5-ML Al film on Pt(111) increased the Al 2s BE by ∼1.5 eV. However, this shift is referenced to the Al emission measured at 300 K, at which temperature the Al is electronically perturbed because of Al/Pt alloying.[4] Comparison with "unalloyed" core-level spectra obtained by film growth at 160 K Al reveals the true shift to be ∼2.0 eV relative to metallic Al and, thus, consistent with Al^{3+} formation. Similar BE shifts have been observed for 300 and 1000 K oxidation of Al films on Ag,[25] Re, and Ru[15,26] substrates and likewise associated with oxidation to Al^{3+}.

The aluminum oxide stoichiometry resulting from 300 K oxidation of submonolayer Al films can be estimated by comparing the O 1s intensity from a 0.25-ML O_a coverage on clean Pt(111) with that obtained from Al-covered surfaces. STM shows these submonolayer deposits form 2D dendritic islands without Al/Pt intermixing.[4] By correcting the O 1s signal from oxidized Al films of 0.25−1.0 ML thickness for the O_a contributions from bare Pt sites, one obtains an average Al:O ratio of 1:1.3, close to that expected for stoichiometric Al_2O_3, suggesting that submonolayer Al films on Pt(111) are almost completely oxidized at 300 K.

Aluminum oxide films grown on single-crystal substrates have been widely studied by HREELS and LEED to determine the crystallinity and nature of oxide phase formed.[15,26,27,28] We found no ordered structures detectable by LEED upon 300 K oxidation of submonolayer Al films. The corresponding HREELS spectra exhibit only very weak losses, again indicating the absence of long-range order. STM reveals oxidation of submonolayer Al films is accompanied by a ~10% expansion, which agrees quantitatively with the attenuation of the Pt photoemission.

A 1100 K annealing of submonolayer alumina films does induce crystallinity as shown by the appearance of a $(4\sqrt{3} \times 4\sqrt{3})R30°$ LEED pattern corresponding to a real space unit mesh having $a = b = 19.3$ Å. This LEED pattern reflects the large unit cell of Al_2O_3 ($a = b = 4.75$ Å, $\alpha = 120°$ [21]), which often results in poor registry of oxide overlayers with the metal substrate and the occurrence of multiple domains.[15, 27,28,29] The resulting diffraction patterns may be further complicated by multiple scattering events. The periodicities deduced from LEED patterns observed for similar AlO_x films on Re(0001), NiAl(110), and Ta(110) have been interpreted in terms of oxygen-anion separations of between 3 and 3.2 Å. These compare with the $O^{2-}-O^{2-}$ separation of ~2.8 Å for bulk Al_2O_3 and presumably reflect substrate-induced distortions of the oxide lattice. On Pt(111) the overlayer unit cell is comparable in size to that observed on Re(0001), and we calculate an oxygen-anion spacing of ~3.2 Å, corresponding to a significantly distorted oxide structure.

For thick oxide films, LEED shows a periodicity of ~2.8 Å corresponding to undistorted alumina. Of course, this is also close to the periodicity characteristic of Pt(111) itself (2.77 Å). However, we associate the (1×1) LEED pattern displayed by thick alumina film with partially disordered alumina rather than with patches of uncovered Pt(111) because under the conditions of our measurements any bare metal surface should be covered by a (2×2) oxygen overlayer.[30]

Since both γ- and α-Al_2O_3 exhibit distinctive vibrational spectra, HREELS measurements assist in identification of the phases formed by oxidation of thick and thin Al deposits. α-Al_2O_3 exhibits two strong fundamental vibrational modes at 496 and 806 cm^{-1},[31] while the calculated spectrum for γ-Al_2O_3 [32] predicts three modes at 400, 658, and 909 cm^{-1}. For the crystalline submonolayer oxide we observe losses at 450, 670, and 870 cm^{-1}, consistent with those calculated for γ-Al_2O_3. Similar observations have been reported for oxidized Al films on Re(0001),[15] NiAl(110),[28] and Mo(110).[33] The same three losses have been observed upon oxidation of Al(111) [34] and assigned to the ν_1, ν_2, and ν_3 vibrations, respectively, of the oxide lattice.[35]

The combined LEED and HREELS results discussed above suggest the following structural model for a thin γ-Al_2O_3 film on Pt(111), in which the morphology of γ-Al_2O_3 is strongly perturbed by the substrate symmetry. For Pt(111), a hexagonal close-packed array of oxygen atoms would be expected to control the registry of an Al_2O_3 overlayer with the substrate.[29] γ-Al_2O_3 has a defect spinel structure and is composed of alternating A and B layers.[36] The A layer consists of mixed octahedrally and tetrahedrally coordinated Al^{3+}, while the B layer is composed of solely octahedrally coordinated Al^{3+} cations. Figure 13 shows a schematic of the A layer of γ-Al_2O_3 superimposed on a Pt(111) surface. The periodicity determined by LEED (Figure 6A) is consistent with an $O^{2-}-O^{2-}$ spacing of 3.2 Å; hence, a single overlayer unit cell will consist of a 6 $\times$ 6 array of O^{2-} anions as shown in Figure 13. Earlier studies

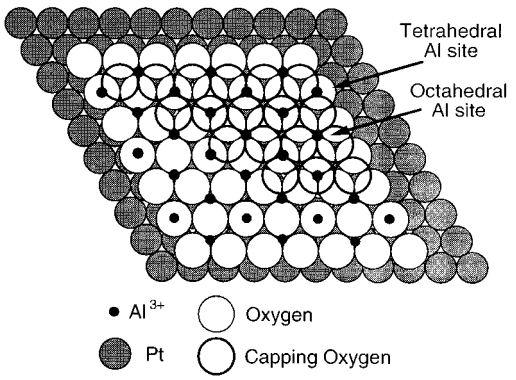

Figure 13. Schematic showing the structure of an oxygen-terminated (111) layer of γ-Al_2O_3 superimposed on Pt(111), resulting in the $(4\sqrt{3} \times 4\sqrt{3})R30°$ periodicity observed in Figure 6. The positions of the O^{2-} anions and octahedrally and tetrahedrally coordinated Al^{3+} cations are illustrated.

of the surface of bulk γ-Al_2O_3 samples[36] and of thin γ-Al_2O_3 films on transition-metal substrates[28] show that the γ-Al_2O_3 surface is O^{2-}-terminated. The observed LEED pattern shown in Figure 6A can be accounted for by the presence of three equivalent domains of the overlayer shown in Figure 13, reflecting the 3-fold symmetry of the substrate surface. For thicker γ-Al_2O_3 films the lattice parameter is expected to tend toward that of bulk Al_2O_3, corresponding to an $O^{2-}-O^{2-}$ spacing of 2.8 Å, which is in accord with our LEED observations for multilayer Al_2O_3 films on Pt(111).

The oxidation kinetics and morphology of 300 K oxidized AlO_x overlayers exhibit a strong dependence on initial Al coverage. The oxygen uptake data in Figure 3 show that although the initial rates of oxidation are comparable for submonolayer and multilayer Al films, the latter oxidize more slowly for exposures above 10 L. Thus, a 50-L O_2 exposure is sufficient to fully oxidize submonolayer Al deposits, at which point the corresponding oxygen signal from a 5-ML Al film has attained only ~75% of its saturation value. These differences result from a combination of factors. At 300 K, multilayer Al films on Pt(111) grow by formation of an Al-rich Al/Pt alloy at the interface, capped by a pure Al overlayer.[5] As noted above, submonolayer films consist of an *unalloyed* Al overlayer.[5] Therefore, initial oxidation of thicker Al deposits involves rapid incorporation of oxygen into the capping Al layer and should mirror the oxygen dissociation and oxide nucleation processes occurring on their submonolayer counterparts. However, with the thick films, higher oxygen exposures induce a large decrease in the Pt 4d intensities (of ~30% for a 5-ML film), strongly suggesting that the additional oxygen uptake observed over such thick Al deposits is associated with Al segregation from the subsurface alloy phase.

Diffusion limitations and the stabilizing influence of interfacial alloying with Pt greatly reduce the rate and degree of thicker film Al oxidation possible at 300 K. (Figure 3 demonstrates that Al atoms in the Pt_3Al surface alloy are extremely unreactive toward oxygen). Thus, although oxygen uptake over thick Al deposits appears to saturate at ~200−300 L, and the Al Auger peak shift from 66 to 58 eV indicates Al^{3+} in the near-surface layers, the less surface-sensitive Al 2s spectra show that ~60% of Al remains in metallic form. Assuming equivalent escape depths for the Al 2s and O 1s electrons (of ~8 Å), if the deconvoluted Al^{3+} 2s:O 1s XP ratio is taken, the stoichiometry of the capping oxide layer can be *estimated*. This gives the same stoichiometry derived for submonolayer films, namely, ~1:1.5, and shows that although low-temperature

treatments cannot fully oxidize multilayer Al films, *the fraction so oxidized exists as stoichiometric Al_2O_3.* Submonolayer Al films, for which a sharp substrate-overlayer interface exists, oxidize more readily and completely at low oxygen exposures and low temperatures.

As with submonolayer oxide films, multilayer oxide films formed at 300 K do not exhibit long-range order. The single HREELS loss feature observed at 660 cm^{-1} can be attributed to a disordered surface oxide, also reported by Chen et al for AlO_x on Mo(110).[34] Our photoemission measurements suggest that this disordered oxide is present as islands as opposed to a continuous film. Thus, for a 5-ML oxidized Al deposit comprising ~40% Al^{3+}, the Pt 4d intensity should attenuate by at least 50% for such a continuous AlO_x film. In fact, the measured attenuation is only 30%. The presence of oxide islands is strongly supported by the observation that CO-titratable Pt sites persist in the presence of oxidized multilayers (Figure 1).

In addition to generating a crystalline product, high-temperature oxidation results in more complete oxidation of Al multilayers. This is clear from the increased O 1s intensity and corresponding loss of metallic Al from the Al 2s region following 800 K oxidation compared with results from the 300 K treatment (Figure 2b). This reflects (i) increased oxygen mobility and (ii) oxidative extraction of Al from the alloy selvedge. The associated HREELS losses at 650 and 820 cm^{-1} are inconsistent with α-Al_2O_3 formation, for which vibrational modes at 496 and 806 cm^{-1} are expected.[27] However, they are in agreement with the losses observed after high-temperature oxidation of thick Al films on Mo(110),[34] which are consistent with γ-Al_2O_3 formation.

Oxidative extraction of Al from the mixed Pt/Al interface eliminates the strong Pt/Al interaction present in the as-deposited film, which arises from Al → Pt charge transfer.[5] This is manifest in both the Pt valence band and Pt 4d XP spectra, which upon oxidation revert to their "clean-surface" condition. Our findings in regard to the AlO_x capping layer are entirely consistent with the behavior observed for Pt clusters deposited on Al_2O_3(1000):[37] 1100 K reduction results in formation of a Pt_3Al interfacial alloy whose subsequent oxidation generates AlO_x clusters on top of the Pt particles. More interestingly, reduction/oxidation of dispersed Pt/Al_2O_3 catalysts[3] also leads to formation of AlO_x atop the Pt particles, which can profoundly affect catalytic properties. Therefore, the present model system should also be useful for the study of such effects.

ii. Reactivity of AlO_x Films. The principal motivation for characterization of the AlO_x/Pt(111) system was to prepare a model catalyst over which the role of Al_2O_3 in SO_2-promoted propane oxidation over conventional Pt/Al_2O_3 catalysts could be studied. Recently, the growth of Al_2O_3 films on refractory metal substrates[38] or NiAl(110) [39] followed by deposition of metal clusters has been shown to provide a realistic model for dispersed catalyst systems. However, in this study an understanding of the interactions at the Pt−Al_2O_3 interface is required in the absence of any structural changes induced by SO_2 [40] that may also influence the chemistry of propane oxidation.[41] Within these constraints, a study using the inverse system described in this paper is more appropriate.

In the absence of SO_2, AlO_x/Pt(111) does not chemisorb propane. Therefore, the reactive properties after SO_2 treatment are attributed to the interaction of SO_2 with both AlO_x/Pt and with bare Pt. Promotion of propane oxidation by SO_2 adsorption is an efficient process that can be followed under UHV conditions over Pt(111) [8] and at high pressure over Pt/Al_2O_3 catalysts.[7] The results presented here demonstrate that the reaction can also be carried out over an SO_2-promoted AlO_x/Pt(111) model catalyst, where submonolayer Al_2O_3 films enhance the yield of oxidation products relative to the yield from clean Pt(111).

The key activating species on Pt(111) has been identified as SO_4.[9] This increases the dissociative sticking probability of propane, probably by H abstraction and formation of an adsorbed alkyl species that undergoes combustion.[8,18] On powdered alumina, SO_2 readily forms $Al_2(SO_4)_3$ at ~420 K.[4] This is stable to >720 K.[17] Our work on Pt(111)[9] demonstrates that adsorbed SO_4 formed on the oxygenated metal by SO_2 uptake is stable to only 550 K, with a maximum coverage of around 0.1 ML. Hence, the presence of alumina on Pt(111) should increase the total SO_4 coverage, as indeed indicated by the S 2p XP spectra in Figure 12.

Given that sulfated Al_2O_3 powder chemisorbs propane,[7] in the present case one might expect additional hydrocarbon uptake on the SO_4-bearing Al_2O_3 films. The resulting organic adspecies might react at the Pt−Al_2O_3 interface by either spillover of hydrocarbon fragments to Pt sites or reverse spillover of atomic oxygen from Pt to Al_2O_3. In either case, bare Pt sites are essential for dissociative chemisorption of O_2; hence, with increasing Al_2O_3 film thickness, the concentration of bare Pt sites decreases correspondingly and the system is expected to become oxygen-deficient. This should favor partial oxidation (CO) over total oxidation (CO_2) with increasing Al_2O_3 film thickness (and thus propane uptake), precisely as observed in Figure 10. The maximum product yield is obtained when the concentration of adsorbed SO_4 and the number of bare Pt sites are optimized. The appearance of a high-temperature SO_2 desorption peak for submonolayer Al_2O_3 films on Pt(111) suggests the presence of an Al_2O_3-stabilized SO_4 species bound at the Pt−Al_2O_3 interface. STM shows that the dendritic nature of the Al_2O_3 islands promotes a high Pt−Al_2O_3 perimeter at which HC/O_a spillover can occur. It is possible that these interfacial perimeter sites are principally responsible for hydrocarbon capture and subsequent reaction with Pt sites. However, the coincidence of CO and CO_2 product desorption peaks observed during propane oxidation over clean[8] and Al_2O_3-covered Pt(111) surfaces suggests a common reaction site; i.e., only spillover of hydrocarbon fragments from Al_2O_3 to Pt sites is important.

With the thickest Al_2O_3 films (which correspond to islands of oxide and patches of bare Pt), the product yield is comparable to that found for the bare Pt (111) surface. This suggests that there must be an oxygen supply in addition to the O_a present on the Pt. Decomposition of the SO_x species at the Pt−Al_2O_3 interface to liberate atomic oxygen could account for this observation. This interpretation is supported by the results presented in Figure 11, which show that as the Al_2O_3 film thickness increases, more SO_x is consumed in the reaction with propane, leading to a decreased SO_3 desorption yield.

The strong promotion of propane oxidation over dispersed Pt/Al_2O_3 catalysts by SO_2 may therefore be rationalized in terms of a bifunctional mechanism involving initial dissociative chemisorption of propane on sulfated Al_2O_3 and O_2 on bare Pt sites. Subsequent reaction of the activated hydrocarbon (most likely an alkyl fragment) and atomic oxygen at the Pt−Al_2O_3 interface results in efficient combustion of propane. Under the true catalytic cycle SO_4 must regenerate after the initial C−H activation step presumably by the reaction of SO_x with atomic oxygen, both of which are continuously replenished from the gas phase over practical Pt/Al_2O_3 automotive catalysts.

Conclusions

(1) At 300 K submonolayer films of Al on Pt(111) undergo complete oxidation to Al_2O_3. Heating to 1100 K results in formation of a somewhat strained crystalline film of γ- alumina. Thicker films undergo incomplete oxidation at 300 K with increased oxidation taking place at 800 K and involving extraction of Al from the initially mixed Pt/Al interface. At high temperatures these thicker oxide films also undergo crystallization, apparently forming undistorted γ-alumina. The crystalline Pt_3Al surface alloy is resistant to oxidation at 300 K but undergoes complete oxidation at 800 K.

(2) Incomplete oxidation of thick Al deposits results in formation of a stoichiometric Al_2O_3 capping layer on top of metallic Al.

(3) Al_2O_3 films on Pt(111) increase both the coverage and stability of SO_4(a) generated by SO_2 chemisorption. This in turn markedly increases the activity of these surfaces for propane oxidation.

(4) Propane oxidation over Al_2O_3/Pt(111) surfaces probably occurs via a bifunctional mechanism in which propane dissociatively chemisorbs on sulfated Al_2O_3 patches followed by spillover of hydrocarbon fragments onto O_a-covered Pt sites at the Pt−Al_2O_3 boundary.

(5) This model planar system provides a useful means of examining aspects of the structural and reactive behavior of dispersed Pt/alumina catalysts.

Acknowledgment. This work was supported under Grant No. GR/K45562 awarded by the U.K. Engineering and Physical Sciences Research Council. We are grateful to Johnson Matthey for a loan of precious metals.

References and Notes

(1) Taylor, K. C. In *Catalysis Science and Technology*; Anderson, J. R., Boudart, M., Eds.; Springer-Verlag: Berlin, 1982; Vol. 5, Chapter 2.
(2) Maire, G. L. C.; Garin, F. G. In *Catalysis Science and Technology;* Anderson, J. R., Boudart, M., Eds.; Springer-Verlag: Berlin, 1984; Vol. 6, Chapter 3.
(3) Den Otter, G. J.; Dautzenberg, F. M. *J. Catal.* **1978**, *53*, 116.
(4) Wilson, K.; Brake, J.; Lee, A. F.; Lambert, R. M. *Surf. Sci*. **1997**, *387*, 257.
(5) Burch, R.; Hayes, M. J. *J. Mol. Catal. A.* **1995,** *100*, 13.
(6) Hubbard, C. P.; Otto, K.; Gandhi, H. S.; Ng, K. Y. S. *J. Catal.*, **1993**, *139*, 268.
(7) Yao, H. C.; Stephien, H. K.; Ghandi, H. S. *J. Catal.* **1981**, *67*, 231.
(8) Wilson, K.; Hardacre, C.; Lambert. R. M. *J. Phys. Chem*. **1995**, *99*, 13755.
(9) Wilson, K.; Hardacre, C.; Baddeley, C. J.; Lüdecke, J.; Woodruff, D. P.; Lambert, R. M. *Surf. Sci.* **1997**, *372*, 279.
(10) Lee, A. F.; Wilson, K.; Lambert, R. M.; Hubbard, C.; Gandhi, H. S. In preparation.
(11) Horton, J. H.; Moggridge, G. D.; Ormerod, R. M.; Kolobov, A. V.; Lambert, R.M. *Thin Solid Films* **1994**, *237*, 134.
(12) Hardacre, C.; Roe, G. M.; Lambert, R. M. *Surf. Sci.* **1995**, *326*, 1.
(13) Wytenburg, W. J.; Lambert, R. M. *J. Vac. Sci. Technol. A* **1992**, *10*, 3597.
(14) Ko, C. S.; Gorte, R. J. *Surf. Sci.* **1985**, *155*, 296.
(15) Wu, Y.; Garfunkel, E.; Madey, T. E. *Surf. Sci*. **1996**, *365*, 337.
(16) Zhou, X. L.; White, J. M. *J. Vac. Sci. Technol* **1993**, *11*, 2210.
(17) Saur, O.; Bensitel, M.; Mohammed Saad, A. B.; Lavalley, J.C.; Tripp, C. P.; Morrow, B. A. *J. Catal.* **1986**, *99*, 104.
(18) Wilson, K.; Hardacre, C.; Lambert, R. M. In *Heterogeneous Hydrocarbon Oxidation*; Warren, B. K., Oyama, S. T., Eds.; ACS Symposium Series 638; American Chemical Society: Washington, D.C., 1996; p 394.
(19) Castro, M. E.; White, J. M. *J. Chem. Phys.* **1991**, *95*, 6057.
(20) Burke, M. L.; Madix, R. J. *Surf. Sci.* **1988**, *194*, 223.
(21) Cocke, D. L.; Johnson, E. D.; Merrill, R. P. *Catal. Rev. Sci. Eng*. **1984**, *26*, 163.
(22) Weast, R. C., Ed. *CRC Handbook of Chemistry and Physics*, 69th ed; The Chemical Rubber CompanyL Cleveland, 1988.
(23) Berg, C.; Raaen, S.; Borg, A.; Andersen, J. N.; Lundgren, E.; Nyholm, R.; *Phys. Rev. B.* **1993**, *47*, 13063.
(24) McConville, C. F.; Seymour, D. E.; Woodruff, D. P.; Bao, S. *Surf. Sci.* **1987**, *188*, 1.
(25) Wytenburg, W. J. Ph.D. Thesis, University of Cambridge, U.K., 1991.
(26) Wu, Y.; Tao, H.-S.; Garfunkel, E.; Madey, T. E.; Shinn, N. D. *Surf. Sci.* **1995**, *336*, 123.
(27) Bardi, U.; Atrei, A.; Rovida, G. *Surf. Sci.* **1992**, *268*, 87.
(28) Jaeger, R. M.; Kuhlenbeck, H.; Freund, H.-J.; Wuttig, M.; Hoffmann, W.; Franchy, R.; Ibach, H. *Surf. Sci.* **1991**, *259*, 235.
(29) Chen, P. J.; Goodman, D. W. *Surf. Sci.* **1994**, *312*, L767.
(30) Gland, J. L.; Sexton, B. A.; Fischer, G. B. *Surf. Sci.* **1980**, *96*, 587.
(31) Liehr, M.; Thiry, P. A.; Pireaux, J. J.; Caudano, R. *J. Vac. Sci. Technol. A* **1984**, *2*, 1079.
(32) Frederick, B. G.; Apai, G.; Rhodin, T. N. *Surf. Sci.* **1991**, *244***,** 67.
(33) Chen, J. G.; Colaianni, M. L.; Yates, J. T. *Phys. Rev. B.* **1990**, *41*, 8025.
(34) Chen, J. G.; Crowell, J. E.; Yates, J. T. *Phys. Rev. B.* **1986**, *33*, 1436.
(35) Erskine, J. L.; Strong, R. L. *Phys. Rev. B.* **1982**, *25*, 5547.
(36) Knözinger, H.; Ratnasamy, P. *Catal. Rev. Sci. Eng.* **1978**, *17*, 31.
(37) Cairns, J.; Boglin, J. E. E.; Clarke, G. J.; Zeigler, J. F. *J. Catal.* **1983**, *83*, 301.
(38) Xu, C.; Oh, W. S.; Liu, G.; Kim, D. Y.; Goodman, D. W. *J. Vac. Sci. Technol. A.* **1997**, *15*, 1261.
(39) Bertrams, T.; Winkelmann, F.; Uttich, T.; Freund, H. J.; Neddermeyer, H. *Surf. Sci.* **1995**, *333*, 1515.
(40) Ebitani, K.; Konno, H.; Tanaka, T.; Hattori, H. *J. Catal*. **1992**, *135*, 60.
(41) Otto, K.; Andino, J. M.; Parks, C. L. *J. Catal.* **1991**, *131*, 243.
(42) Mitchell, M. B.; Sheinker, V. N.; White, M. G. *J. Phys. Chem.* **1996**, *100*, 7550.